Axial buckling of multiwall carbon nanotubes with heterogeneous boundaries

F. M. Tong, C. Y. Wang,[a] and S. Adhikari
School of Engineering, Swansea University, Singleton Park, Swansea, Wales SA2 8PP, United Kingdom

(Received 24 October 2008; accepted 29 March 2009; published online 11 May 2009)

The finite element method has been employed to study the effects of different boundary conditions on the axial buckling of multiwall carbon nanotubes (MWCNTs). Unlike previous works, both homogeneous and heterogeneous end constraints are considered for the constituent tubes of various MWCNTs comprising shell-type (i.e., the length-to-diameter ratio $L/D<10$), beam-type (i.e., $L/D>10$), and the two different types of constituent tubes. The results show that clamping the individual tubes of simply supported or free MWCNTs exerts a variety of influences on their buckling behaviors depending on the type of the MWCNTs, the position, and the number of the clamped tubes. Clamping the outermost tube can enhance the critical buckling strain up to four times of its original value and can shift the buckling modes of those MWCNTs consisting both shell- and beam-type tubes. In contrast, little difference can be observed when simply supported ends of MWCNTs are replaced by free ends or vice versa. Explicit buckling mode shapes obtained using the finite element method for various physically realistic cases have been shown in the paper. © *2009 American Institute of Physics*. [DOI: 10.1063/1.3125312]

I. INTRODUCTION

Buckling or structural instability forms a fundamental consideration in the mechanics of carbon nanotubes (CNTs) due to the slender and thin walled nature of their structure. In the last two decades, intensive studies have been performed to achieve an in-depth understanding on this issue.[1] As reviewed in Ref. 1, such an investigation was first focused on the fundamental buckling case of CNTs.[2–5] The effect of the interlayer van der Waals (vdW) interaction is a major issue for the buckling of multiwalled CNTs (MWCNTs).[6] One of the basic findings is that for relatively stocky MWCNTs with, e.g., the innermost radius-to-thickness ratio $R_i/H \leq 1/4$ (Refs. 7–9) and the length-to-the-outermost-diameter ratio $L/D_o<10$,[10] the effect of the interlayer vdW interaction is limited due to the high radial rigidity of the individual tubes. Here H is the effective thickness, L is the length, R_i is the innermost radius, and D_o is the outermost diameter. In this case, the buckling is initiated on the outermost (or a few outer) layer(s) while other inner layers still remain stable.[4,5,7] The "infinitely" strong effect of the vdW interaction occurs for thin [e.g., $R_i/H \geq 5$ (Refs. 6, 8, and 9)] and slender [e.g., $L/D_o>10$ (Ref. 10)] MWCNTs with low radial rigidity of their constituent tubes. In these MWCNTs, the interlayer vdW interaction can resist the change in the interlayer spacing, leading to an efficient load transfer between neighboring tubes in radial direction. As a result, all constituent tubes of such MWCNTs will buckle simultaneously with an identical radial (or transverse) displacement. It has been shown that under the axial compression thin MWCNTs ($R_i/H \geq 5$) and slender MWCNTs ($L/D_o>10$) will buckle like single-layer thin shells[7,8] and hollow Euler beams,[10] respectively.

These interesting results also reveal the prominent dimensional effect on the buckling of MWCNTs which has been further studied in details in Refs. 4, 7, and 11–13. Other factors that could have significant influences on the buckling of CNTs, e.g., boundary condition,[14,15] defects of CNTs,[16,17] and thermal effect,[18–21] have also been identified recently. The effect of boundary condition on CNT buckling is of practical interest as CNTs are expected to be building blocks of a vast range of engineering nanostructures, where the surrounding materials will inevitably impose different types of constraints on the ends of CNTs. Previous work has already shown that the critical buckling load of single wall CNT (SWCNTs) (Ref. 14) and double wall CNT (DWCNTs) (Ref. 15) increases considerably when their simply supported ends are replaced by clamped ones. Nevertheless, this issue has not been examined for MWCNTs of more than two layers. Moreover, in all previous buckling analyses,[4–15] MWCNTs are always assumed to have homogeneous boundary condition, i.e., the same boundary condition is specified on all the constituent tubes of MWCNTs. This assumption, used to simplify the analysis, may not be always true in many engineering applications of CNTs. MWCNTs are coupled systems of its constituent tubes via the interlayer vdW interaction. The individual tubes, thus, could play substantially different roles in stabilizing the mechanical structures of the MWCNTs. As a result, the overall buckling behaviors of MWCNTs could be very sensitive to the boundary condition of some tubes but indifferent with others. In view of this discussion, it is of great interest to conduct a detailed study on the effect of boundary condition on the buckling of MWCNTs by considering homogeneous and heterogeneous boundary conditions.

In the present study, we focus on the axial buckling of six types of MWCNTs. i.e., (1) very thin ($R_i/H \geq 5$), (2) thick ($R_i/H \approx 1$), (3) almost solid ($R_i/H \leq 1/4$), (4) short ($L/D_0 \leq 5$), (5) intermediate ($L/D_0 \approx 10$), and (6) long

[a]Electronic mail: chengyuan.wang@swansea.ac.uk.

MWCNTs ($L/D_0 \geq 20$). Subsequently, three sets of boundary conditions, i.e., free, simply supported, and clamped, have been assigned to individual tubes to explore the unique buckling response of these MWCNTs with different end constraints. In order to conduct a systematic buckling analysis of MWCNTs with various homogeneous and heterogeneous boundary conditions, the finite element (FE) method has been employed. The multilayer elastic shell model for MWCNTs[6,8,9,11] widely used in the previous studies is further extended to the proposed buckling analysis.

II. FE MODEL FOR THE BUCKLING OF MWCNTS

MWCNTs comprise two to dozens layers of coaxial constituent single wall tubes. The individual tubes are coupled via the interlayer vdW interaction in radial direction.[6] The friction between neighboring tubes is usually very low and, thus, has been neglected in the present study. The model and mathematical strategies used in the present work for the axial buckling analysis of MWCNTs are described and validated in this section.

A. Model and analysis method

To study the mechanical behaviors of MWCNTs, Ru[6,22,23] developed a multiple-elastic shell model with good agreement with available experiment[8] and molecular dynamic simulations.[11,24,25] Following Ru,[6,22,23] each constituent tube of MWCNTs will be modeled as an elastic shell with equivalent wall thickness h, Young's modulus E, and Poisson ratio ν. When deformation occurs, the vdW interaction between two adjacent tubes is calculated by $p=c\cdot(w_0-w_i)$ and the interaction between the other (nonadjacent) tubes as well as the interlayer friction is ignored. Here, w_0 and w_i denote the radial displacements of the outer and inner tubes of two adjacent tubes, respectively. The constant c is the vdW interaction coefficient defined by the second derivative of the interlayer potential energy with respect to the interlayer spacing. The value of c at the equilibrium interlayer spacing of 0.34 nm is estimated as $c=102$ GPa/nm.[11,26] The mathematical strategy formulated by Ru[6,22,23] for the MWCNTs with simply supported ends cannot be employed directly in the present study where MWCNTs with various homogeneous and heterogeneous boundary conditions are considered. To circumvent this problem, a FE technique has been developed based on the methodology suggested by Wang *et al.*[15] The solid shell element is adopted, and the mesh design is selected such that each tube of MWCNTs consists of 36 elements in the cross sectional area and $45L/10R_i$ elements in the longitudinal direction. The vdW interactions between adjacent tubes are simulated by linear springs of stiffness $k=(c/2)(A_i+A_o)$, where A_i and A_o are the midareas of the inner and outer elements, respectively. Obviously, the stiffness k is a constant for a specific tube but varies between different individual tubes. For more details regarding the FE modeling technique, reader may refer to Ref. 15. In Fig. 1, a typical full FE model for a five-wall CNT is illustrated in a global Cartesian system (x,y,z). Here, the ANSYS FE software package is used to perform the buckling analysis of MWCNTs.

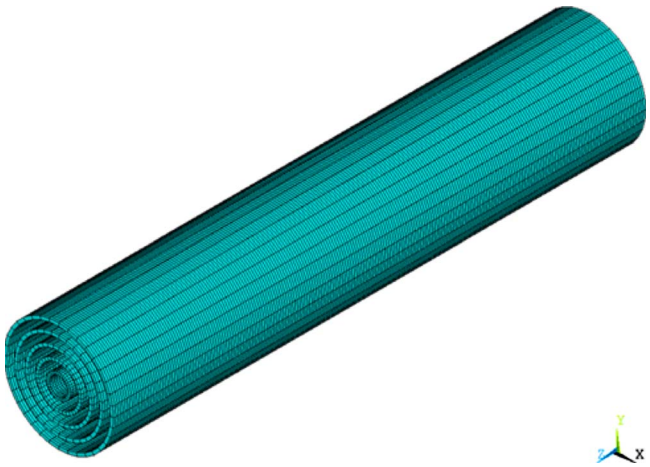

FIG. 1. (Color online) A typical element mesh of a five-wall CNT.

In the present buckling analysis of MWCNTs, the two ends of each constituent single wall CNT are subjected to one of the following three sets of boundary conditions.

(1) The free (F) boundary conditions: $u=0$.
(2) The simply supported (SS) boundary condition: $u=0$, $v=0$, and $w=0$.
(3) The clamped (C) boundary conditions: $u=0$, $v=0$, $w=0$, and $dw/dx=0$.

Here u, v, and w are the displacements of the individual tubes in longitudinal, circumferential, and radial directions, respectively. In the FE analysis, imposing the clamped boundary condition on CNTs is straightforward and can be done by constraining the nodes of the CNT end(s) for displacements and rotations. The simply supported ends of solid cylinders can also be achieved simply by restricting the tangential displacement of the concentric end nodes while allowing their rotation about any axes. This method, however, is not applicable for hollow CNTs where nodes do not exist in the concentric axis. To solve this problem, we shall introduce an imaginary plane at the end of CNTs, which encloses the hollow CNTs and enables the aforementioned constraint to be applied to its concentric nodes, thus reflecting a simply supported end of CNTs. Ideally, the free boundary condition implies that only the loading direction (i.e., axial direction) is constrained, without any restriction imposed on the rotation and displacements in the transverse directions. Unfortunately, in the FE analysis such an end constraint leads to the floating and/or twisting of CNTs and gives rise to premature nonconvergence of the solution. To avoid this problem, some constraints have to be applied in all three principle axis (i.e., x, y, and z axes in Fig. 1). In the present analysis, the true free end of MWCNTs is replaced by constraints which could represent it as closely as possible, Here a minimal tangential constraint has been applied on the innermost tube. Consequently, the so-called free boundary condition of MWCNTs considered in this study reflects a simply supported boundary condition for the innermost tube and free boundary condition for other outer tubes. Here, it is emphasized that this consid-

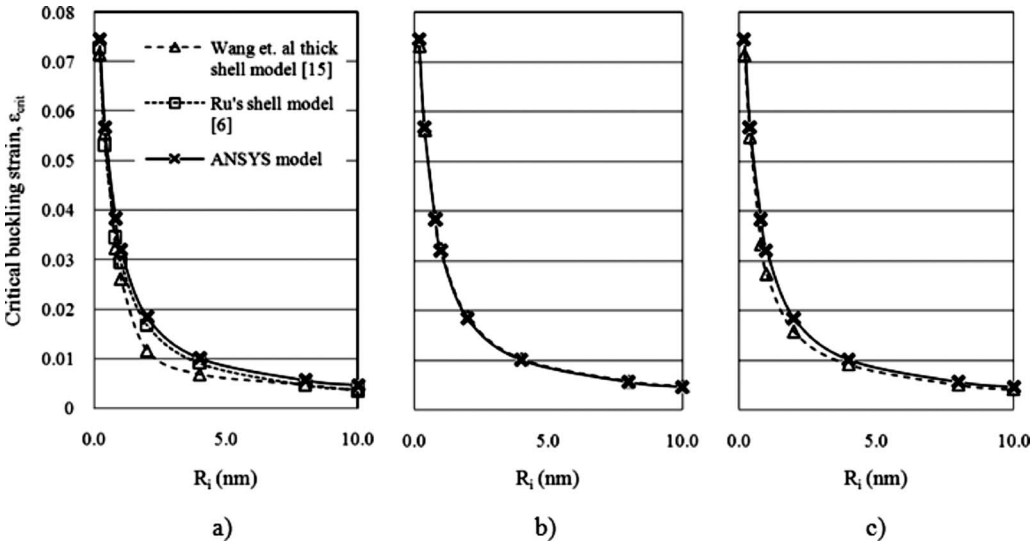

FIG. 2. Comparison of the critical buckling strains predicted by different models for DWCNTs with constant length-to-the-inner-radius ratio $L/R_i=10$ and three sets of boundary conditions, i.e., (a) SS-SS, (b) SS-C, and (c) C-C.

eration is only necessary when we consider MWCNTs in a homogeneous free constraint state, i.e., all constituent tubes are subject to free boundary condition.

B. Validation of the model

The ANSYS model for the buckling of MWCNTs is developed based on the FE techniques of Wang *et al.*[15] Nevertheless, the software and the methods to impose the boundary conditions used here could be different from those employed in Ref. 15. This could lead to discrepancies between the two studies. To ensure that the ANSYS model gives a reliable description to the buckling behaviors of CNTs we shall compare it with the model of Wang *et al.*[15] in predicting the critical buckling strain of DWCNTs. Following Ref. 15, three sets of end constraints, namely, (a) two ends simply supported (SS-SS), (b) one end simply supported, and one end fixed (SS-C) and (c) two ends clamped (C-C), are considered. Two groups of DWCNTs, namely, (1) DWCNTs of $R_i=0.3$ to 10 nm and $L/R_i=10$ and (2) DWCNTs of $L/R_i=5$ to 100 and $R_i=0.4$ nm have been used in this study. For the sake of comparison we consider Young's modulus $E=5.5$ TPa, Poisson's ratio $\nu=0.19$, and the effective thickness $H=0.066$ nm for single wall CNTs. These values are taken from Ref. 15. The critical buckling strains given by the ANSYS model are shown in Figs. 2 and 3 and compared with those predicted by the model of Wang *et al.*[15] The results given by Ru's thin shell model[22] and the Euler beam model[27] are also included for comparison where appropriate.

It can be seen from Figs. 2 and 3 that the ANSYS model is generally in good agreement with the model of Wang *et al.*[15] for the buckling of DWCNTs. In the case of slender DWCNTs of $L/R_i>20$, our results in Fig. 3 almost coincide with the results of Wang *et al.*[15] for all the three sets of boundary conditions considered. When L/R_i exceeds 40, as shown in Fig. 3, the Euler beam model also matches the ANSYS model and the model of Wang *et al.*[15] This implies

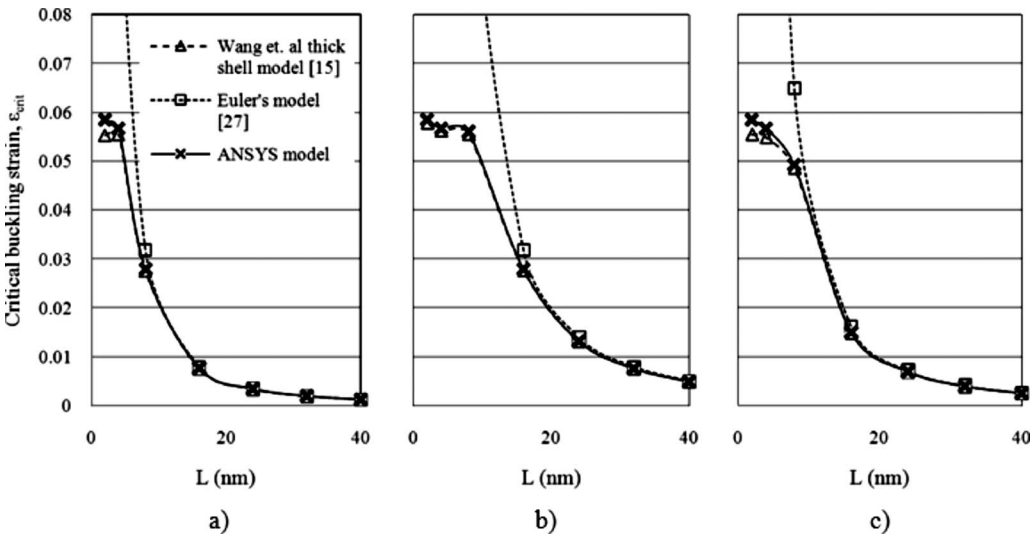

FIG. 3. Comparison of the critical buckling strains predicted by different models for DWCNTs with constant inner radius $R_i=0.4$ nm and three sets of boundary conditions, i.e., (a) SS-SS, (b) SS-C, and (c) C-C.

TABLE I. Five-wall CNTs as typical examples of MWCNTs considered in the present study.

Examples	1 (Thin)	2 (Thick)	3 (Solid /short)	4 (Solid/intermediate)	5 (Solid/long)
R_i (nm)	6.8	1.36	0.34	0.34	0.34
H (nm)	1.36	1.36	1.36	1.36	1.36
L (nm)	81.6	27.2	17	34	68
$L/(D_0)$	5	5	5	10	20
R_i/H	5	1	0.25	0.25	0.25

that in the axial buckling a slender DWCNT behaves like a hollow Euler beam where buckling occurs in the axial direction with a rigid body motion of its circular cross section. For relatively stocky DWCNTs with $L/R_i \leq 10$, the discrepancies between the ANSYS model and Wang *et al.*'s model can be observed in Figs. 2 and 3. Such discrepancies, however, are small and generally less than 10%. Larger discrepancies of 20% to 58% are found only in a narrow range of R_i, approximately given by $R_i=1.5-4$ nm, when SS-SS ends are considered [Fig. 2(a)]. It can be seen from Fig. 2 that, for this particular case, the ANSYS model is always in accordance with Ru's[22] thin shell model. This thin shell model is accurate for thin DWCNTs of $R_i/H>4$ and incorporates mathematically exact simply supported boundary conditions. Thus, the aforementioned large discrepancy between the ANSYS model and the model by Wang *et al.*[15] is probably a result of different approximate methods used to simulate the simply supported boundary condition for hollow CNTs.

III. BUCKLING OF MWCNTS UNDER AXIAL COMPRESSION

In what follows, we use the ANSYS model to examine the effects of boundary conditions on the axial buckling of MWCNTs. The examples of five-wall CNTs (see Table I) studied here can be classified into six categories, i.e., (1) thin (example 1), (2) thick (example 2), (3) almost solid (example 3) MWCNTs with the innermost radius-to-thickness ratio R_i/H decreasing from 5, 1 to 0.25, (4) short (example 3), (5) intermediate (example 4), and (6) long (example 5) MWCNTs with the length-to-the-outermost-diameter ratio L/D_0 increasing from 5, 10 to 20. Two types of boundary conditions are imposed on the five examples: (i) homogeneous boundary condition where the constituent tubes of MWCNTs have identical end constraints, and (ii) heterogeneous boundary condition where some individual tubes are subject to different end conditions. The values of equivalent material and geometric constants of SWCNTs used in the present study are Young's modulus $E=3.5$ TPa, the effective wall thickness $H=0.1$ nm, and Poisson ratio $\nu=0.2$.[28,29]

A. Homogenous boundary conditions

We first consider homogeneous boundary conditions for the five examples in Table I. For homogeneous boundary conditions all the constituent tubes of MWCNTs have the same end constraints. Based on the ANSYS model, the buckling modes are shown in Fig. 4 for the five examples with free (F-F), simply supported (SS-SS), and clamped (C-C) boundary conditions. The corresponding critical buckling strains ε_{cr} are shown in Figs. 5(a) and 5(b) for examples 1, 2, and 3, and Examples 3, 4, and 5, respectively. Recall that the simulation of a homogeneous F-F boundary condition is not ideal but considered "close" to the real free end constraints and has been included in this study as a reference.

It can be seen from Fig. 4 that examples 1 and 2 (for which $L/D_O=5$) exhibit shell-like buckling characterized by localized wall bending along the circumferential and/or lon-

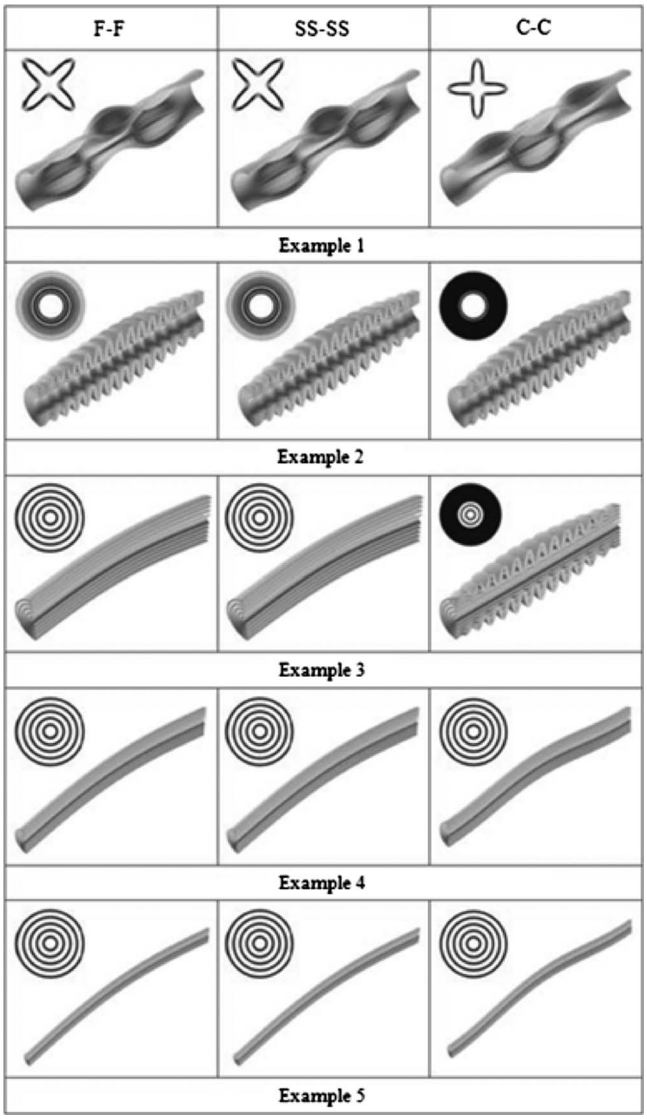

FIG. 4. The buckling modes for the five examples of Table I under homogeneous free (F-F), simply supported (SS-SS), and clamped (C-C) boundary conditions. The corresponding cross-sectional deformation at the midlength is also shown for each buckling mode.

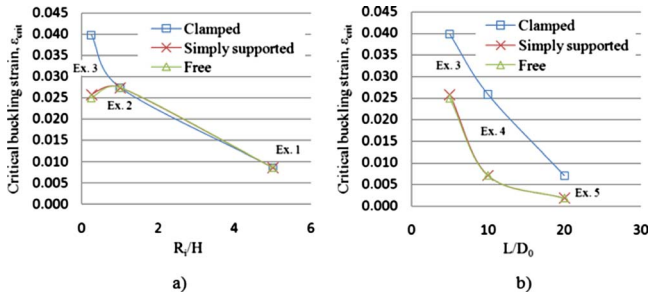

FIG. 5. (Color online) The critical buckling strains calculated as functions of (a) the inmost radius-to-thickness ratio R_i/H for examples 1, 2, and 3 of Table I, and (b) the length-to-the-outermost-diameter ratio L/D_0 for examples 3, 4, and 5 of Table I. Here, three sets of boundary conditions shown in the figure are considered.

gitudinal directions. In this case, the axial buckling mode (Fig. 4) and the associated critical buckling strain ε_{cr} [Fig. 5(a)] do not change significantly with the three sets of boundary conditions. However, they vary considerably with the ratio R_i/H. Example 1 with $R_i/H=5$, i.e., a thin MWCNT, displays the bulging of the shell wall where the deformation occurs in both longitudinal and circumferential directions. The bulging observed for Example1 shows long axial wavelengths (Fig. 4) and low critical buckling strain ε_{cr} of 0.0086 [Fig. 5(a)]. When R_i/H decreases to unity, a ripplelike buckling occurs for example 2, with the wall bending mainly observed in the longitudinal direction. The buckling of example 2 is characterized by shorter axial wavelengths (Fig. 4) and higher critical buckling strain ε_{cr} of 0.0274 [Fig. 5(a)]. More detailed study reveals that the radial displacements of thin MWCNTs (example 1) are almost identical for all the constituent tubes. This suggests that the interlayer vdW interaction can efficiently resist the change in the interlayer spacing of thin MWCNTs whose radial rigidity is very low. Thus, as shown in Fig. 4, example 1 behaves as if it were a single-layer elastic thin shell. This observation is consistent with the previous prediction based on Ru's[6] multiple-thin shell model and the molecular mechanics model of Chang *et al.*[7] Such an effect of the interlayer vdW interaction becomes less pronounced for thick MWCNTs (example 2) due to their higher radial rigidity. Thus, the radial displacement of example 2 is found to decrease from the outermost tube to the innermost one, which leads to significant changes in the interlayer spacing between the adjacent tubes (see the cross sections in Fig. 4).

In contrast to the cases of example 1 (a thin MWCNT) and example 2 (a thick MWCNT), strong effects of boundary condition have been observed for example 3 of $R_i/H=0.25$ and $L/D_O=5$ [a (almost) solid and short MWCNT]. As seen from Fig. 4, example 3 with C-C ends remains a ripplelike buckling mode similar to that of example 2. Nevertheless, when the F-F or SS-SS boundary condition is imposed, the beamlike buckling can be observed. This is evident from the global bending along the longitudinal direction and a rigid body motion of the circular cross section. Accordingly, Fig. 5 shows that the critical buckling strain ε_{cr} of example 3 with C-C ends is much greater than those obtained for the lower degree end constrains, i.e., F-F or SS-SS. Here, it is noted that the constituent tubes of example 1 have (almost) identical length-to-diameter aspect ratio of 5. Thus all of these tubes can be treated as typical elastic shells. In the case of example 2, the aspect ratio of the individual tubes increases from 5 (for the outermost tube) to 10 (for the innermost tube), showing that most of the constituent tubes can still be modeled as shells. Naturally, examples 1 and 2 exhibit the shell-like buckling under axial compression. For example 3, the aspect ratio of the innermost tube is 25, which is five times that of the outermost tube. In other words, while the outermost tubes remain a typical shell-type structure, the innermost tube turns out to be an equivalent long beam. These constituent tubes of substantially different aspect ratios, however, tend to buckle in a uniform pattern due to the strong coupling of the adjacent tubes via the vdW interaction. This unique feature of example 3 results in a "competition" between the beamlike and the shell-like buckling. As consequence we can observe strong effects of the boundary condition on the buckling behaviors in example 3. It may be also observed from Fig. 4 that the constituent tubes of example 3 buckle simultaneously in the beamlike mode. However, at the onset of the shell-like buckling, only a few outer tubes deform while the innermost two tubes remain nearly unreformed with negligible displacements.

Now we study examples 4 and 5 with the aspect ratio L/D_O increasing from 10 to 20 as shown in Table I. These two five-wall CNTs are considered as typical examples of intermediate and long MWCNTs, respectively. Here the constituent tubes of examples 4 and 5 are of a large aspect ratio ranging from 10 to 100, i.e., they have typical beam-type structures. As can be observed in Fig. 4, no matter what boundary condition is applied, these two examples always bucklelike elastic beams with circular cross sections and unchanged interlayer spacing. In Fig. 5(b), the critical buckling strains ε_{cr} of clamped examples 4 and 5 are nearly four times as much as those obtained for simply supported conditions. These results for slender MWCNTs are similar to the analytical prediction for Euler beams, which is explained by the variation of their equivalent length due to the change in the end constraints.[27] On the other hand, in Figs. 4 and 5, replacing SS-SS boundary condition with the F-F one does not make any observable difference for the buckling of all the five examples in Table I. It is thus concluded that the axial buckling of MWCNTs is only sensitive to the restriction on the rotation of their two ends.

B. Heterogeneous boundary conditions

In this section we study the axial buckling of MWCNTs with heterogeneous boundary conditions where constituent tubes have different end constraints. We sequentially clamp the constituent tubes of a MWCNT with simply supported and free boundary conditions until all the constituent tubes are clamped. This clamping procedure is carried out in the following two separate sequences: (1) to clamp the outermost tube first, then its adjacent tube, and finally the innermost tube, which is denoted by (O-I), and (2) to clamp the innermost tube first, then the next tube, and finally, the outermost tube, which is represented by (I-O). We use the notation (A) to denote the change from SS-SS to C-C boundary

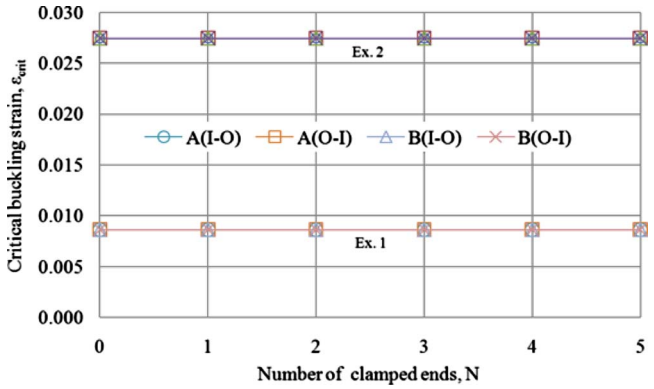

FIG. 6. (Color online) The critical buckling strains of examples 1 and 2 with respect to the number of clamped tubes N in the four cases, i.e., A(O-I), A(I-O), B(O-I), and B(I-O).

condition and notation (B) to denote the change from F-F to C-C boundary condition. The following four cases are considered in the present study: A(O-I), A(I-O), B(O-I), and B(I-O). The dependence of ε_{cr} on the number of clamped tubes N is calculated for the four cases and plotted in Figs. 6 and 7 for examples 1–5.

As seen in Sec. II A, examples 1 and 2 consist primarily of short constituent tubes with small aspect ratios and show shell-like buckling. This buckling mode is insensitive to the boundary condition change from homogeneous SS-SS or F-F to homogeneous C-C. Thus, as expected, in Fig. 6 ε_{cr} of examples 1 and 2 is almost a constant independent of the position and the number of clamped tubes. Examples 4 and 5, however, are made up of long constituent tubes of large aspect ratios. As a result, they display the beamlike buckling (Fig. 4) for all boundary conditions considered here. It is observed in Fig. 7 that ε_{cr} for examples 4 and 5 rises considerably with the number of clamped tubes. When the outermost one or two tubes are first clamped, i.e., $N=1$ to 2, for cases A(O-I) and B(O-I), ε_{cr} increases rapidly toward its maximum possible value. However, further clamping the inner tubes until the fully clamped state increases ε_{cr} only slightly. In the cases A(I-O) and B(I-O), i.e., fix the innermost tube first, ε_{cr} grows gradually with the number N and reaches its maximum value only when the MWCNTs are fully clamped. From these results it follows that clamping

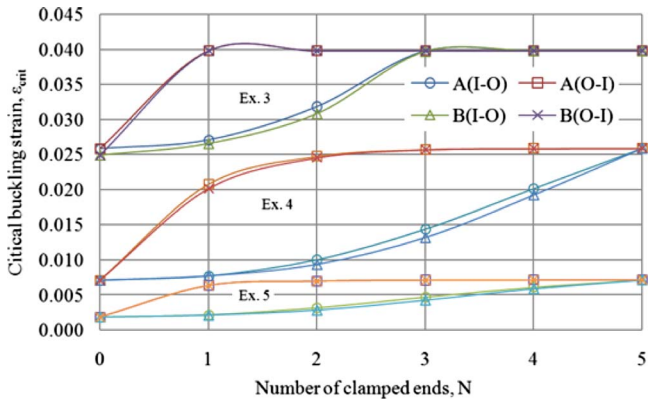

FIG. 7. (Color online) The critical buckling strains of examples 3, 4, and 5 with respect to the number of clamped tubes N in the four cases, i.e., A(O-I), A(I-O), B(O-I), and B(I-O),

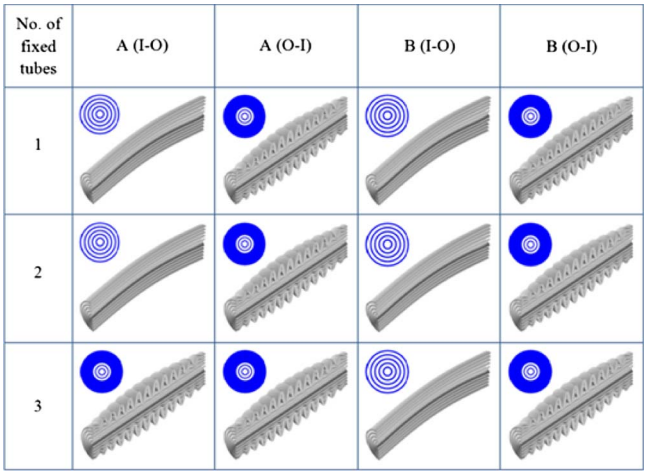

FIG. 8. (Color online) The axial buckling modes of example 3 of Table I at the number of clamped tubes $N=1$, 2, and 3 for the four cases, i.e., A(O-I), A(I-O), B(O-I), and B(I-O).

the outermost tube can efficiently enhance ε_{cr} of slender MWCNTs up to its possible maximum value. This maximum value associated with the fully clamped state is nearly four times of ε_{cr} obtained for the SS-SS and F-F boundary conditions.

Similar results for ε_{cr} can also be observed in Fig. 7 for example 3 which is a mixture of shell-type outermost tubes and beam-type innermost tubes. The buckling of example 3 could switch between the beamlike mode and shell-like mode depending on the imposed boundary conditions. In Fig. 4, all the tubes of example 3 with SS-SS or F-F ends buckle simultaneously in the beamlike mode. This implies that with SS-SS or F-F ends the influence of the innermost beam-type tube is predominant, which, via the interlayer vdW interaction, can even force a few shell-type outermost tubes to buckle in the beamlike mode. However, once the outermost tube is fixed, for the cases A(O-I) and B(O-I), the original beamlike buckling changes into the shell-like buckling as shown in Fig. 8. Accordingly, ε_{cr} increases rapidly in Fig. 7. The clamped outermost tube and the next two tubes of example 3 buckle like elastic thin shells whereas the two beam-type innermost tubes are still in a stable state. With further clamping of the inner tubes, example 3 retains the same buckling mode (Fig. 8) and an almost identical critical buckling strain ε_{cr} (Fig. 7). If the innermost one to three tubes of example 3 are fixed first, the beamlike mode remains unchanged (Fig. 8) and accordingly ε_{cr} increases progressively for cases A(O-I) and B(O-I) (Fig. 7). When the fourth tube is fixed, i.e., $N=4$, the shell-like buckling occurs (not shown in Fig. 8) with ε_{cr} almost equal to its maximum value corresponding to $N=5$. These results reveal that clamping the outermost layer can efficiently prevent the beamlike bucking of the innermost tube(s) and result in shell-like buckling of a few outer tubes with higher critical buckling strain ε_{cr}. In this particular case, the innermost slender tube(s) still stay stable at the onset of shell-like buckling. The possible explanation is that for the innermost beam-type tube, the critical strain of the shell-wall buckling could be much higher than those of a few shell-type outer tubes.

MWCNTs usually have sealed two ends. Thus, it is more realistic to impose the desired boundary condition on their outermost tube. According to the above results, the axial buckling of MWCNTs is most sensitive to the restriction on the rotation of their two ends, i.e., clamped end constraint. Clamping the outermost tube is nearly equivalent to fixing all the constituent tubes, which can enhance the critical buckling strain up to four times of the value associated with homogeneous SS-SS or F-F boundary conditions. These interesting findings, indeed, provide guidance for the design of CNT-based engineering nanostructures. Possible examples are CNT-reinforce nanocomposites[30] and MWCNT tip of atomic force microscopes,[31] where the axial buckling strain is one of the major concerns. On the other hand, it should be pointed out that the present model is developed for individual MWCNTs of constant interlayer spacing of 0.34 nm. It does not account for the influence of variable interlayer spacing in abnormal MWCNTs (Ref. 32) and the interaction between CNTs and surrounding media.[33] The effects of boundary condition on the buckling of abnormal MWCNTs or the MWCNTs on substrates could be different from what has been obtained in the present study.

IV. CONCLUSIONS

The FE method has been used to examine the effects of boundary condition on the axial buckling of MWCNTs. The homogeneous and heterogeneous boundary conditions have been considered for six types of MWCNTs. The examples include thin, thick, and (almost) solid MWCNTs defined by $R_i/H \geq 5$, ≈ 1, and ≤ 0.25, respectively, and short, intermediate, and long MWCNTs defined by $L/D_o \geq 5$, ≈ 10, and ≥ 20, respectively. The major conclusions arising from the present study are summarized as follows.

(1) The axial buckling of MWCNTs is generally sensitive to the restriction of the rotation at the two ends. Accordingly, clamping the constituent tubes could have high impacts on their buckling behaviors. The variation between the free and simply supported boundary conditions does not exert significant influence on the buckling of MWCNTs.
(2) The effect of clamping the constituent tubes of originally simply supported or free MWCNTs is sensitive to (i) the geometrical features of MWCNTs and (ii) the position and the number of the clamped tubes.

(a) Thin or thick MWCNTs (e.g., examples 1 and 2 of Table I) consisting of SWCNTs with relatively small aspect ratios, say smaller than 10, always buckle in shell-like modes which are insensitive to the change of the boundary conditions of the MWCNTs.
(b) Slender MWCNTs (e.g., examples 4 and 5 of Table I) comprising SWCNTs with large aspect ratios, say larger than 10, show beamlike buckling for all the boundary conditions considered here. The critical buckling strain rises significantly with the increasing number of clamped tubes. Clamping only the outmost tube can raise the critical buckling strain significantly. In our studies we found that it can be up to four times of its original value.
(c) Almost solid and short MWCNTs (e.g., example 3 of Table I) are a combination of the outermost shell-type tubes of small aspect ratios, say 5, and the innermost beam-type tubes of large aspect ratios, say 25. In this case, free and simply supported boundary conditions lead to the beamlike buckling associated with a low critical buckling strain. Imposing the clamped end constraint on the outmost layer can transform the buckling into the shell-like mode and efficiently enhance the critical buckling strain toward its maximum possible value.

It is expected that these findings will be important for the conceptual design of nanostructures consisting MWCNTs.

[1] C. Y. Wang, Y. Y. Zhang, C. M. Wang, and V. B. C. Tan, J. Nanosci. Nanotechnol. **7**, 4221 (2007).
[2] B. I. Yakobson, C. J. Brabec, and J. Bernholc, Phys. Rev. Lett. **76**, 2511 (1996).
[3] S. Iijima, C. Brabec, A. Maiti, and J. Bernholc, J. Chem. Phys. **104**, 2089 (1996).
[4] A. Sears and R. C. Batra, Phys. Rev. B **69**, 235406 (2004).
[5] K. M. Liew, C. H. Wong, X. Q. He, M. J. Tan, and S. A. Meguid, Phys. Rev. B **69**, 115429 (2004).
[6] C. Q. Ru, J. Appl. Phys. **89**, 3426 (2001).
[7] T. C. Chang, W. L. Guo, and X. M. Guo, Phys. Rev. B **72**, 064101 (2005).
[8] C. Y. Wang, C. Q. Ru, and A. Mioduchowski, J. Nanosci. Nanotechnol. **3**, 199 (2003).
[9] C. Y. Wang, C. Q. Ru, and A. Mioduchowski, Int. J. Solids Struct. **40**, 3893 (2003).
[10] C. Q. Ru, Phys. Rev. B **62**, 16962 (2000).
[11] C. Y. Wang and A. Mioduchowski, J. Appl. Phys. **101**, 014306 (2007).
[12] Y. Y. Zhang, C. M. Wang, and V. B. C. Tan, J. Appl. Phys. **103**, 053505 (2008).
[13] A. G. Arani, R. Rahmani, A. Arefmanesh, and S. Golabi, J. Mech. Sci. Technol. **22**, 429 (2008).
[14] P. S. Das and L. T. Wille, Comput. Mater. Sci. **24**, 159 (2002).
[15] C. M. Wang, Y. Q. Ma, Y. Y. Zhang, and K. K. Ang, J. Appl. Phys. **99**, 114317 (2006).
[16] H. Xin, Q. Han, and X. H. Yao, Carbon **45**, 2486 (2007).
[17] X. Hao, H. Qiang, and Y. Xiaohu, Compos. Sci. Technol. **68**, 1809 (2008).
[18] H. S. Shen and C. L. Zhang, Phys. Rev. B **74**, 035410 (2006).
[19] X. H. Yao and Q. Han, ASME J. Eng. Mater. Technol. **128**, 419 (2006).
[20] C. L. Zhang and H. S. Shen, Phys. Rev. B **75**, 045408 (2007).
[21] H. S. Shen and C. L. Zhang, Int. J. Solids Struct. **44**, 1461 (2007).
[22] C. Q. Ru, J. Appl. Phys. **87**, 7227 (2000).
[23] C. Q. Ru, J. Mech. Phys. Solids **49**, 1265 (2001).
[24] C. Y. Wang, C. Q. Ru, and A. Mioduchowski, ASME J. Appl. Mech. **71**, 622 (2004).
[25] C. Y. Wang, C. Q. Ru, and A. Mioduchowski, Phys. Rev. B **72**, 075414 (2005).
[26] C. Y. Wang, C. Q. Ru, and A. Mioduchowski, J. Appl. Phys. **97**, 024310 (2005).
[27] S. Timoshenko and J. M. Gere, *Theory of Elastic Stability* (McGraw-Hill, New York, 1961).
[28] C. Y. Wang and L. C. Zhang, Nanotechnology **19**, 075705 (2008).
[29] C. Y. Wang and L. C. Zhang, Nanotechnology **19**, 195704 (2008).
[30] K. T. Lau and D. Hui, Composites, Part B **33**, 263 (2002).
[31] D. P. Burt, N. R. Wilson, J. M. R. Weaver, P. S. Dobson, and J. V. Macpherson, Nano Lett. **5**, 639 (2005).
[32] K. M. Liew, J. B. Wang, X. Q. He, and H. W. Zhang, J. Appl. Phys. **102**, 053511 (2007).
[33] J. Xiao, H. Jiang, D.-Y. Khang, J. Wu, Y. Huang, and J. A. Rogers, J. Appl. Phys. **104**, 033543 (2008).